Combined theoretical and experimental kinetic approach for methane conversion on model supported Pd/La0.7MnO3 NGV catalyst: Sensitivity to inlet gas composition and consequence on the Pd-support interface

Yuanshuang Zheng, Amaury Decoster, Andrea Osti, Antonella Glisenti, Jean-Philippe Dacquin, Fabien Dhainaut, Svetlana Heyte Dyshlovenko, Pascal Granger

Submitted to the Journal of Catalyst as Priority communication/Research note

Combined theoretical and experimental kinetic approach for methane conversion on model supported $Pd/La_{0.7}MnO_3$ NGV catalyst : Sensitivity to inlet gas composition and consequence on the Pd-support interface

Yuanshuang Zhang[1], Amaury Decoster[1], Andrea Osti,[1,2] Antonella Glisenti,[2,3] Jean-Philippe Dacquin[1], Fabien Dhainaut[1], Svetlana Heyte[1], Pascal Granger[1]*

[1] *Univ. Lille, CNRS, Centrale Lille, ENSCL, Univ. Artois, UMR 8181 - UCCS - Unité de Catalyse et Chimie du Solide, F-59000 Lille, France*
[2] *Dept. of Chemical Sciences, University of Padova, Via F. Marzolo, 1, 35131, Padova, Italy*
[3] *CNR-ICMATE, INSTM, Via F. Marzolo, 1, 35131, Padova, Italy*

Corresponding author : Email : pascal.granger@univ-lille.fr
Phone number : +33 320 434 938

Abstract

New insights into reaction mechanism for catalytic methane combustion are provided in broad operating conditions on $Pd/La_{0.7}MnO_3$ as model natural gas vehicle catalyst. Under lean conditions and dry conditions a dual mechanism is suggested with active site combining reactive oxygen species from $La_{0.7}MnO_3$ and palladium sites. Aging in wet atmosphere has no consequence on the kinetic behavior. On the other hand, in wet atmosphere near the stoichiometry, strong accumulation of OH groups on the support would suppress the metal-support interface. Accordingly, methane combustion would take place only on Pd particles

.

Keywords : Methane combustion, NGV three-way catalyst, Palladium, perovskite, kinetics

1. Introduction

At short term, the substitution of liquid fuels by natural gas powered engines is envisioned and complies with more stringent regulations on atmospheric pollutant emissions with lower NO_x and nearly no particulates emission. However, more efficient three-way catalytic technologies must be developed to avoid unburnt methane emission recognized as greenhouse gas. One of the key issue lies in their weak efficacy near the stoichiometry or under slightly rich exposure typically under three-way catalytic operating conditions. Up to now the kinetics of methane combustion and related model prediction has been investigated essentially in lean conditions on bentchmark supported palladium catalysts [1-5]. Numerical simulations near stoichiometric conditions from relevant microkinetic analysis are scarce [6,7]. A critical factor lies in the preservation of the metal dispersion of PdO_x species recognized as the active sites in stoichiometric/rich atmosphere [8,9]. At high temperature typically encountered in three-way operating conditions, the decomposition of PdO_x into less active nanometric metallic Pd^0 species cannot be strictly ruled out causing a loss of efficiency. [8]. Presently, there is no clear consensus on the nature and architecture of active sites in typical three-way operating conditions. Miller and Malatpure [10] assumed a pair site composed of PdO and Pd^0. New generation of three-way catalysts has arisen in the past two decades able for stabilizing the dispersion of precious metals in a broader temperature range under switching lean/rich exposure thanks to strong interactions with perovskite structures [11-13]. The development of such supported catalysts has also opened the debate with no longer unanimity by simply considering PdO_x as the active site of the reaction. For instance, Lu et al. [14] synthesized hexagonal Pd-$YFeO_{3\pm\delta}$ structure by flame-spray-pyrolysis, with preferential formation of supported Pd^0 and Pd^{2+} species instead of solid solution. They observed a strong rate enhancement in methane conversion after cycling up to 850°C under reaction conditions assigned to the formation of metallic particles and the phase transition to

orthorhombic $YFeO_{3\pm\delta}$. Gonzáles-Marcos et al. [15] also observed the coexistence of two kinetic regimes from light-off curves on Pd supported on $Ce_{0.68}Zr_{0.32}O_2$ explained by the involvement of Pd(+I)-like species at low temperature while metallic Pd^0 species would act as active sites at high temperature. Different kinetic regimes have been also identified on Pd/Al_2O_3-CeO_2 assigned to the prevalence of the Pd-Ce or Pd-PdO interface accompanied with higher TOF values and lower activation barrier in the former case [16]. The existing controversies on the nature of active sites related reaction mechanisms lies also on the presence or the absence of water in the inlet feed gas. Steam has currently a detrimental effect [17] by hindering oxygen mobility on the support and suppressing the oxygen exchange process at the metal support interface [18]. In addition water can originate deactivation because of strong accumulation of water of the support weakening the strenght of Pd nanoparticles with the support material and then becoming more sensitive to coalescence process inducing changes in the particle size and morphology.

This study reports a kinetic study of the catalytic CH_4/O_2 reaction in the presence and in the absence of steam on pre-reduced and aged $Pd/La_{0.7}MnO_3$ catalysts. Different reaction mechanisms have been compared based on combined theoretical and experimental approaches that account for single and dual sites involving surface reactive oxygen species form the perovskite. It will be found that the richness of the inlet gas composition in the presence and in the absence of steam has strong impact on the nature of active sites and related reaction mechanism. On the other hand a good stability was found upon aging process.

2. Materials and methods

Two reproducible batches have been prepared by using a classical citrate route for the preparation of La-deficient $La_{0.7}MnO_3$ perovskite support material. La-deficiency was found

to improve oxygen storage properties [19,20]. Calcination in air led to the formation of the pure orthorhombic structure with no discernible bulk impurities due to single oxide segregation. 1 wt.% palladium was incorporated through a classical wet impregnation by using palladium nitrate as precursor salt. The impregnated solid precursor was subsequently dried in air at 100°C and calcined in air at 400°C. Hydrogen titration was performed at 100°C according to a pulse technique to measure the metal dispersion assuming H/Pd =1. Prior chimisorption measurements, the samples were pre-reduced at 250°C in hydrogen. For the two samples comparable Pd dispersions were obtained of 3.1% and 2.1%.

Catalytic measurements were carried out on the REALCAT plaform in a Flowrence high-throughput unit supplied by Avantium. Flowrence unit is equipped with 16 parallel quartz fixed-bed microreactors (d=2mm) and a sampling system composed of a 16-ports multi position valve that enables online gas phase analysis of the products of reaction of each reactor using an Agilent 7890 gas chromatograph. Each microreactor were filled with 30 mg catalyst with average grain size of 100 μm. Steady-state experiments were performed with inlet gas mixture composed of 750-3000 ppm CH_4 with 5 vol.% O_2 in the presence or in the absence of 10 vol.% H_2O in the temperature range 350-600°C. Two similar series were performed first on pre-reduced samples and on aged samples after exposure at 750°C to a mixture composed of 5 vol% O_2 and 10 vol.% H_2O. The second set of steady-state rate measurements were performed in the presence of steam with 750-3000 ppm CH_4, O_2 2000-6000 ppm O_2 and 0.5-2 vol.% H_2O. Prior to catalytic measurements, the catalyst was pre-reduced in hydrogen at 250°C to insure a quasi-complete reduction of PdO to metallic Pd species in agreement with H_2-Temperature-programmed reduction experiments (not shown). For all experiments the space velocity was maintained constant at 10^2 $L.h^{-1}.g^{-1}$. Calculation of the Weisz-Prater criterion as detailed in Supplementary Information (SI) suggested that kinetic measurements were performed in chemical regime.

3. Results and discussion

3.1. Theoretical approach on model Pd(111) surface

The unity bond index-quadratic exponential potential (UBI-QEP) is a theoretical method suited for straigthforward calculations of heat and activation energies for elementary steps involved in a catalytic reaction according to a thermodynamic approach described in SI. This method can be considered as a generalization of the bond order conservation Morse potential method as described elsewhere [21]. Calculations of activation barrier E and enthalpy of reaction ΔH were performed on a closed-packed Pd(111) surface with preferred three-fold hollow sites. As explained in SI, only gas phase total bond energy (D) and atomic heat of chemisorption (Q) are needed [22]. Numerical values are listed in Fig. 1(a) and account for a typical accuracy of 5-15 kJ/mol. These values correspond to the zero-coverage limit when free sites are largely available, which is rarely the case when catalytic measurements are performed near atmospheric pressure. The heat of adsorptions for not activated adsorption processes, *i.e.* dissociative and molecular adsorption respectiviely for O_2 and CH_4, reveal a much higher exothermicitiy of oxygen adsorption reflecting a stronger adsorption. Subsequent surface reactions have been considered with two different scenarios for the dissociation of chemisorbed methane molecules involving a nearest-neigbor vacant Pd site or occupied by chimisorbed O atoms. Slightly lower activation barrier is obtained in the former case (97 kJ/mol vs. 117 kJ/mol) which emphasizes that chemisorbed O would not *a priori* favor the C-H bond breaking in $CH_{4,ads}$ molecules in these coverage conditions. Previous DFT calculations on PdO(101) surface [23] differ from these conclusion showing that hydrogen abtraction from methane would occur more readily over a Pd_{cus}-O_{cus} site pair. As a matter of fact such differences were expected as already pointed out by Zhu et al [3] who found significant change of the activation energy on Pd metal and PdO for methane combustion

suggesting different reaction mechanisms and we must aslo keep in mind the bordeline case for $\theta = 0$ which does not reflect the adsorbate composition in our operating conditions. The intermediate production of CO can be discussed near stoichiometric conditions when the surface is oxygen depleted because it also strongly adsorbs and, similarly to O_{ads} and OH_{ads}, could potentially play the role of inhibitor preventing methane dissociation. Results near zero-coverage *a priori* suggest a detrimental effect of oxygen related to inhibiting effect. However, the adsorbate coverage dependency of the activation barrier assigned to the C-H bond breaking step must be envisioned.

Reaction	ΔH (kJ/mol)	E_f^a (kJ/mol)
$O_2 + 2* \leftrightarrows 2O*$	-232	0
$CH_4 + * \leftrightarrows CH_4*$	-90	0
$CH_4* + * \leftrightarrows CH_3* + H*$	88	97
$CH_3* + * \leftrightarrows CH_2* + H*$	66	104
$CH_2* + * \leftrightarrows CH* + H*$	35	99
$CH* + * \leftrightarrows C* + H*$	-145	21
$C* + O* \leftrightarrows CO* + *$	-174	31
$CO* \leftrightarrows CO + *$	134	-134
$CO* + O* \leftrightarrows CO_2 + 2*$	-36	20
$O* + H* \leftrightarrows OH* + *$	29	90
$OH* + H* \leftrightarrows H_2O + 2*$	-114	0
$2OH* \leftrightarrows H_2O + O* + *$	-144	144
$CH_4* + O* \leftrightarrows CH_3* + OH*$	117	117
$CH_3* + O* \leftrightarrows CH_2* + OH*$	95	102
$CH_2* + O* \leftrightarrows CH* + OH*$	64	93
$CH* + O* \leftrightarrows C* + OH*$	-116	42

[a] forward reaction

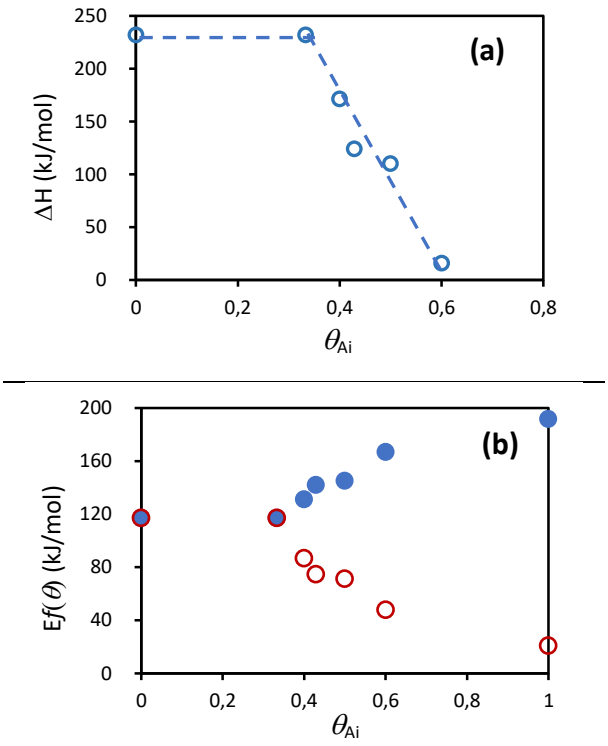

Fig. 1. Heat of reation and activation barrier calculated on Pt(111) at $\theta = 0$. (a), surface oxygen and OH coverage dependency of enthalpy of adsorption for gaseous O_2 (blue) and H_2O (red) (b) surface oxygen and OH coverage dependency of activation barrier of step (13) O coverage (blue) and OH coverage (red)

More representative energetic data can be calculated from the UBI-QEP method upon addition of a coadsorbate originates from the fact that the surface metal atoms interact with more than one adsorbate. O- and OH-coverage dependencies of the adsorption enthalpy and activation barrier are illustrated in Figs 1(a) and 1(b). The decrease in the heat of adsorption at increasing coverage is correctly predicted by the UBI-QEP method. In this study, the

coverage effect of O ad-atom or OH ad-specie is significant considering their heat of adsorption (360 kJ/mol for O ad-atom and 165 kJ/mol for OH ad-specie regardless the surface metal Pd atom). This effect becomes significant when the adsorbed species occupied more than 40% adsorption sites with a sharp weakening effect of Pd-O adsorption bond. The effect of coverage adsorbate can be also quantified on the activation barrier. Particular attention has been paid to the following step $CH_{4*} + O_* \leftrightarrows CH_{3*} + OH_*$ characterized by an activation barrier higher than step corresponding to C-H bond breaking on a nearest-neighbour vacant site. Chemisorbed O atom and OH groups appear as reactant and product respectively. Evolution of the activation with respect to θ_O and θ_{OH} is a key information. Some restrictions in the UBI-QEP method lies in the lack of possibility to consider the mutual interactions between adsorbed O and OH. Figs. 1(a) and (b) only take the repulsive interaction between the same adsorbate, *i.e.* O_{ads} or OH_{ads}, into account. As seen, antagonistic evolutions appear as increasing O-coverage induces a lowering of the activation barrier for θ_O above 0.4. This tendency emphasizes a clear assistance of oxygen in the the C-H bond scission and seems to reconcile previous investigations which privileged a cooperative effect of Pd^0 and PdO [10]. On the contrary, an increase of the activation barrier is observable with a rise of θ_{OH} which clearly shows a detrimental effect. On the basis of these theoretical calculations the classical beneficial effect of nearest neighbour O atoms is restored at increasing coverage while he did not appear formally at nil coverage.

3.2. Kinetics and related reaction mechanism on $Pd/La_{0.7}MnO_3$ in lean conditions

Kinetic parameters calculated on pre-reduced and aged catalyst in 750-3000 ppm CH_4 and 5 vol.% O_2 at 400°C are reported in Table 2. Their comparison with previous studies either on metallic or oxidic Pd surface did not reveal significant discrepancies [4,5,24]. Indeed, an increase of the activation energy on metallic surface is noticeable and the kinetics

obeys to a positive reaction order with respect to methane. The lowering of TOF values in the presence of 10 vol.% H_2O is also consistent with a strong inhibiting effect of water on the reaction rate. Let us note that comparable specific rates and TOF values are measured on aged catalyst still in the absence of water. This observation does not show significant detrimental effect of the aging process. As a matter of fact, previous investigations revealed that the alteration of the metal-support interaction may depend on the nature of the pretreatment and the richness of the reactant mixture with an alteration accentuated in reducing atmophere by using perovskite as substrate [25,26]. Indeed, pre-reduction at moderate temperature, *i.e.* 250°C would prevent the metal support interface.

In first approximation, two reaction mechanisms (I(a) and I(b)) have been examined based on the UBI-QEP method which account for metallic Pd sites stabilized on $La_{0.7}MnO_3$. Mechanism I(b) can be supported due to a combined effect related to a weaker oxygen inhibiting effect associated to a lowering of the heat of adsorption and a lowering of the activation energy of step (13) at increasing O-coverage as expected in large excess of oxygen.

Mechanism I(a)

(1) $O_2(g) + 2* \leftrightarrows 2O_*$
(2) $CH_4(g) + * \leftrightarrows CH_{4*}$
(3a) $CH_{4*} + * \rightarrow CH_{3*} + H_*$
(4a) $CH_{3*} + * \rightarrow CH* + H*$
(5a) $CH_{2*} + * \rightarrow CH* + H*$
(6a) $CH_* + * \rightarrow C* + H*$
(7) $C_* + O_* \rightarrow CO_* + *$
(8) $CO_* + O* \rightarrow CO_2 + 2*$
(9) $2OH_* \rightarrow H_2O + O_* + 2*$

Mechanism I(b)

(1) $O_2(g) + 2* \leftrightarrows 2O_*$
(2) $CH_4(g) + * \leftrightarrows CH_{4*}$
(3b) $CH_{4*} + O_* \rightarrow CH_{3*} + OH_*$
(4b) $CH_{3*} + O_* \rightarrow CH_{2*} + OH_*$
(5b) $CH_{2*} + O_* \rightarrow CH_* + OH_*$
(6b) $CH_* + O_* \rightarrow C_* + OH_*$
(7) $C_* + O_* \rightarrow CO_* + *$
(8) $CO_* + O_* \rightarrow CO_2 + 2*$
(9) $2OH_* \rightarrow H_2O + O_* + 2*$

Mechanism II

(1) $O_2(g) + 2* \leftrightarrows 2O_*$
(2) $CH_4(g) + * \leftrightarrows CH_{4*}$
(3c) $CH_{4*} + \textit{'O'} \rightarrow CH_{3*} + \textit{'OH'}$
(4c) $CH_{3*} + \textit{'O'} \rightarrow CH_{2*} + \textit{'OH'}$
(5c) $CH_{2*} + \textit{'O'} \rightarrow CH_* + \textit{'OH'}$
(6c) $CH_* + \textit{'O'} \rightarrow C_* + \textit{'OH'}$
(7) $C_* + O_* \rightarrow CO_* + *$
(8) $CO_* + O_* \rightarrow CO_2 + 2*$
(10) $2\ \textit{OH'} \rightarrow H_2O + \textit{'O'}$

As a matter of fact, the aforementioned elementary steps closely mimic those already reported in the literature on PdO [13] even though the nature of oxygen can be questioned coming from dissociative adsorption into chemisorbed O species on PdO/Pd and/or surface oxygen lattice species. Mechanism I(a) and I(b) agree with a single site mechanism only composed of Pd atoms with competitive adsorptions of O_2 and methane. The positive reaction order for CH_4 concentration (see Table 1) accounts for the kinetic limiting effect of the first C-H bond dissociation [27]. Fujimoto et al. [5] also suggested that subsequent C-H bond breaking are kinetically insignificant. By assuming the first C-H bond breaking slow, then all the other step would occur much faster and reversible adsorptions can be assumed quasi equilibrated leading to Eqs. (11) and (12) corresponding to surface coverages of adsorbed methane molecules and O atoms, *i.e.* $\theta^*_{CH_4}$ and $\theta^*_O$with θ^*_v corresponding to the fraction of vacant sites based on the hypothesis that O_{ads}, and $CH_{4,ads}$ are the most abundant intermediates at the surface.

$$\theta^*_O = \sqrt{\mathrm{K_O P_{O_2}}}\,\theta_v \quad (11)$$

$$\theta^*_{CH_4} = \mathrm{K}_{CH_4}\mathrm{P_{CH_4}}\,\theta_v \quad (12)$$

$$\text{with } \theta^*_v = \frac{1}{1+\mathrm{K}_{CH_4}\mathrm{P_{CH_4}}+\sqrt{\mathrm{K_O P_{O_2}}}} \quad (13)$$

The expression of the reaction rate in Eqs. (14) and (15) respectively for mechanism I(a) and I(b) can be easily derived in agreement with this set of assumptions.

$$r = k_{3a}\theta^*_{CH_4}\theta^*_v = \frac{k_{3a}K_{CH_4}P_{CH_4}}{\left[1+\mathrm{K}_{CH_4}\mathrm{P_{CH_4}}+\sqrt{\mathrm{K_O P_{O_2}}}\right]^2} \quad (14)$$

$$r = k_{3b}\theta^*_{CH_4}\theta^*_O = \frac{k_{3b}K_{CH_4}P_{CH_4}\sqrt{\mathrm{K_O P_{O_2}}}}{\left[1+\mathrm{K}_{CH_4}\mathrm{P_{CH_4}}+\sqrt{\mathrm{K_O P_{O_2}}}\right]^2} \quad (15)$$

The linear transformed of the reation rate Eqs. (14) and (15) allow a graphical discrimination. In practice, the set of assumptions for their establishment is valid if the ~~plots~~ plots $\sqrt{P_{CH_4}/r}$ and $\sqrt{P_{CH_4}\sqrt{P_{O_2}}/r}$ vs. P_{CH_4} is linear with a positive slope. As a matter of fact a

poor agreement is obtained from the plots in Fig. S1. On the basis of these observations, a dual site mechanism II has been suggested as alternative which differs from Mechanism I(a) and I(b) by the nature of reactive oxygen species. Indeed, they would no longer come from the direct gaseous O_2 dissociative adsorption on metallic Pd sites but from surface lattice oxygen of the perovskite support at the Pd-$La_{0.7}MnO_3$ interface. Let us note that one cannot strictly rule out reactive oxygen species coming from PdO at the vicinity of Pd^0 site eventhough it accepted that oxidation of metallic Pd particle is a slow process [2]. The following Eq. (16) can be derived based on the mathematical development given in SI.

$$r = k_{3c}\theta^*_{CH_4}\theta_O = \frac{k_{3c}\theta^*_{CH_4}(2k_{10}+4k_{3c}\theta^*_{CH_4})}{2k_{10}}\left[1 \pm \sqrt{1-\left(\frac{2k_{10}}{2k_{10}+4k_{3c}\theta^*_{CH_4}}\right)^2}\right] \quad (16)$$

θ_O stands for fraction of surface lattice oxygen oxygen species coming $La_{0.7}MnO_3$, k_n stands for the rate constant for step (n), K_{A_i} and P_{A_i} are respectively the equilibrium constants and the partial pressures for the reactant A_i. By assuming step (3c) as slow step, *i.e.* $k_{10} \gg k_{3c}$, then $\frac{2k_{10}}{2k_{10}+4k_{3c}\theta^*_{CH_4}} \sim 1$, then one can obtain the following simplified Eq. (16).

$$r = \frac{k_{3c}K_{CH_4}P_{CH_4}}{(1+K_{CH_4}P_{CH_4}+\sqrt{K_oP_{O_2}})}\left[1 + \frac{2k_{3c}K_{CH_4}P_{CH_4}}{k_{10}(1+K_{CH_4}P_{CH_4}+\sqrt{K_oP_{O_2}})}\right] \quad (17)$$

Kinetic and thermodynamic constants in Table 2 have been estimated from a least square method through the minimization of the sum of the square difference between predicted and experimental reaction rates $\sum(r_{exp.} - r_{predic.})^2$. Only Eq. (17) has been considered for the adjustment. The comparison of optimized values obtained on pre-reduced catalyst and after aging at 750°C in steam agree with mechanism II. They corroborate previous conclusions emphasizing the supply of reactive oxygen from the support [17,18]. The rate constant k_{3c} for methane dissociation increases significantly on the aged catalyst which is in agreement with

the decrease of the apparent activation energy from 136 kJ/mol to 97.9 kJ/mol on aged sample (Table 1). Such evolution could suggest a strenghening of the metal support interface. This assumption is supported by comparable values for k_{10} which still indicate a fast restoration of *'O'* reactive species. Such changes also coincide with an alteration of the adsorptive properties of palladium because adsorption competition becomes more in favor of oxygen on aged sample with sharp increase in O-coverage at the expense of methane coverage as illustrated in Fig. 2. Hence, statistically the probability to find adsorbed methane on Pd at the vicinity of reactive O species from perovskite would lessen. This inhibiting effect would exert a diluting effect and counterbalance the increase observed on the reaction rate constant k_{3c} which could potentially explain unchanged specific reaction rate and TOF values on aged $Pd/La_{0.7}MnO_3$. Neverthless, the most prominent information given by those data is related to the absence of deterioration of the Pd-support interface when the catalyst is exposed to 5 vol.% O_2 and 10 vol.% H_2O at 750°C.

3.2. Kinetics and related reaction mechanism on $Pd/La_{0.7}MnO_3$ near the stoichiometry in the presence of steam

The kinetics has been studied near stoichiometric conditions in the 1-2 vol.% H_2O with partial pressure . Consequently, water adsorption must be considered according to the following step (18):

$$H_2O + O_* + * \leftrightarrows 2OH_* \quad (18)$$

By assuming this step quasi at equilibrium then the OH-coverage expression can be expressed according to Eq. (19) :

$$\theta_{OH}^{*} = \left[K_{H_2O} P_{H_2O} \sqrt{K_O P_{O_2}}\right]^{0.5} \theta_v^{*} \quad (19)$$

$$\text{with } \theta_v^{*} = \frac{1}{1 + K_{CH_4} P_{CH_4} + \sqrt{K_O P_{O_2}} + \left[K_{H_2O} P_{H_2O} \sqrt{K_O P_{O_2}}\right]^{0.5}} \quad (20)$$

Regarding the reaction rate Eqs. (14)-(16) their expression only differ from the denominator which includes the following additionnal terms $\left[\mathrm{K}_{H_2O}\mathrm{P}_{\mathrm{H}_2O}\sqrt{\mathrm{K}_\mathrm{O}\mathrm{P}_{\mathrm{O}_2}}\right]^{0.5}$. By examining the reaction order, the positive value with respect to the partial pressure of oxygen seems to invalidate Eqs. (14) and (17) (see Fig. S2 in SI). As a matter of fact, the adjustment routine by using Eq. (17) converge to $K_O = 0$ when the minimum is reached. The best fit is obtained with Eq. (20) with optimized values for the rate constant and equilibrium constant reported in Table 2.

$$r = k_{3b}\theta^*_{CH_4}\theta^*_O = \frac{k_{3b}K_{CH_4}P_{CH_4}\sqrt{\mathrm{K}_\mathrm{O}\mathrm{P}_{\mathrm{O}_2}}}{\left[1+\mathrm{K}_{CH_4}\mathrm{P}_{\mathrm{CH}_4}+\sqrt{\mathrm{K}_\mathrm{O}\mathrm{P}_{\mathrm{O}_2}}+\left[\mathrm{K}_{H_2O}\mathrm{P}_{\mathrm{H}_2O}\sqrt{\mathrm{K}_\mathrm{O}\mathrm{P}_{\mathrm{O}_2}}\right]^{0.5}\right]^2} \quad (20)$$

Hence, near the stoichiometry, in the presence of steam, mechanism I(b) would prevail at the expense of mechanism (II). This means that the Pd-$La_{0.7}MnO_3$ interface in these conditions would be suppressed and only Pd active sites would run in these operating conditions. This could be explained by a strong OH group accumulation onto the support in the presence of steam in the inlet gas mixture blocking mobility and reactivity of surface oxygen lattice. Indeed, Shwartz et al. found on Pd-based catalyst that OH accumulation on the support hinder oxygen mobility and provokes deactivation [17,18]. Despite higher reaction temperature, the value for k_{3b} seems to be abnormally low compared to that calculated in dry conditions at lower T. The opposite trend observed on the apparent activation energy would likely reflect change in the reaction mechanism. By comparing the equilibrium constant and the resulting coverages, it seems obvious θ^*_{OH} remains below the critical coverage value causing a decrease in the rate constant (Fig. 1(c)) and should not exert detrimental effect. The comparison of methane- and O- coverage seems consistent with the absence of oxygen inhibiting effect in agreement with the positive order with respect to oxygen and the prevalence of step (3c) for modeling the reaction rate.

In summary, the Pd-$La_{0.7}MnO_3$ interface would occur in the absence of steam and would be resistant in severe aging conditions ~~aging~~, *i.e.* at 750°C in 5 vol.% O_2 and 10 vol.% H_2O. However, in wet condition, the kinetics is strongly altered due to strong OH accumulation on the support. The deterioration of oxygen mobility and the suppression of Pd-support interface cause deactivation. These observation pause the question on the strategy to optimize the interface of nano-sized Pd particle with support material exhibiting oxygen storage properties for methane conversion based on the detrimental effect of steam.

Table 1. Kinetic parameters for the CH_4/O_2 and $CH_4/O_2/H_2O$ reaction on $Pd/La_{0.7}MnO_3$ respectively in lean and near stoichiometric conditions

Catalyst	Thermal treatment	$p(CH_4)/10^{-3}$ (atm)	$p(O_2)/10^{-3}$ (atm)	$p(H_2O)/10^{-3}$ (atm)	T (°C)	Preexponential factor A (s^{-1})	E_{app} (kJ/mol)	Reaction order CH_4	Reaction order O_2	Reaction order H_2O	Specif. rate $mol.s^{-1}g^{-1}$	TOF (s^{-1})	Reference
1 wt.%$Pd/La_{0.7}MnO_3$	Pre-reduced/250°C	0.75-3.0	50	-	400	6.2×10^{11}	136.0	0.7	-	-	4.5×10^{-8}	0.015	This study
		1	50	100	400			1.7	-	-	0.9×10^{-8}	0.003	This study
	Aged[a]	0.75-3.0	50	-	400	6.4×10^{8}	97.9	0.8	-	-	4.4×10^{-8}	0.015	This study
		1	50	100	400				-	-	2.1×10^{-8}	0.007	This study
	Pre-reduced/250°C	0.75-3.0	2.0-6.0	5.0-20.0	460	2.6×10^{8}	87.6	0.8	0.14	~ –0.8	17.4×10^{-8}	0.088	This study
0.86 wt.% Pd/ZrO_2	Calc./air, 500°C	20	200	1-150	280	-	-	1.1	0.1	-1.0		0.015	[5]
7.7 wt.%$Pd/Si\text{-}Al_2O_3$	Calc./air, 500°C	20	200	-	280	-	85					0.012	[4]
Pd foil	under reaction mixture/500°C	0.2	200	0.0125	280	-	125	0.7	0.2	-0.9		0.59	[24]

[a] in 10 vol.% H_2O in O_2 vol.% at 750°C

Table 2. Kinetic and thermodynamic constants optimized from a least square method at 400°C on $Pd/La_{0.7}MnO_3$

Operating conditions	Thermal treatment	T(reaction) (°C)	k_{3c}[c]	k_{10}[c]	k_{3b}[c]	K_{CH4}[d]	K_O[d]	K_{H2O}[d]
750-3000 ppm CH_4, 5 vol.% O_2	Reduced[a]	400	2.5×10^{-6}	5.2×10^{-2}		17.2	0.05	
	Aged[b]	400	11.6×10^{-6}	2.3×10^{-2}		5.7	0.8	
750-3000 ppm CH_4, 2000-6000 ppm O_2,	Reduced[a]	460			1.0×10^{-5}	94.8	131.8	0.5

[a] pre-reduction at 250°C - [b] aging at 750°C in air with 10 vol.% H_2O

[c] $mol.s^{-1}g^{-1}$ - [d] atm^{-1}

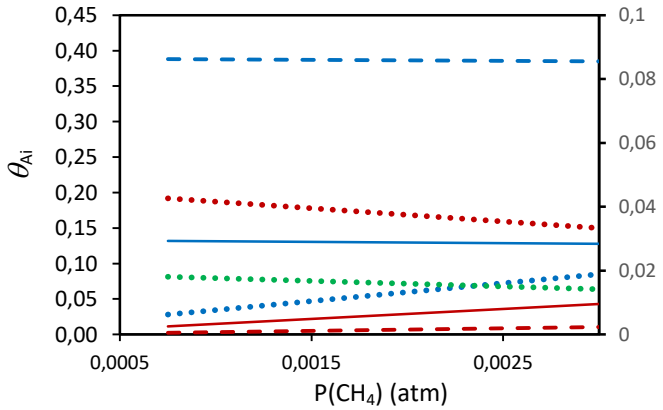

Fig. 2. Evolution of surface coverages θ_{Ai} for methane (red curve), oxygen (blue curve) and OH species (green) vs. methane partial pressure during the CH_4/O_2 reaction on pre-reduced $Pd/La_{0.7}MnO_3$ (bold line), on aged catalyst (- - - -) and on pre-reduced catalyst in the absence of steam and in the presence of steam (**….**).

Acknowlegments

This work was financially supported by the French National Research Agency through the project ANR-18-CE07-0040. One of the co-author (Y. Zheng) was able to benefit from a thesis grant within the framework of this program.

The REALCAT platform is benefiting from a Governmental subvention administrated by the French National Research Agency (ANR) within the frame of the 'Future Investments' program (PIA), with the contractual reference 'ANR-11-EQPX-0037'. The Nord-Pas-de-Calais Region and the FEDER are acknowledged for their financial contribution to the acquisition of the equipment of the platform.

Reference

[1]. J. Au-Yeung, K. Chen, A.T. Bell, E. Iglesia, J. Catal. 188 (1999) 132-139 ;
[2] H. Stotz, L. Maier, A. Boubnov, A.T. Gremminger, J.D. Grundwaldt, O. Deutschmann, J. Catal. 370 (2019) 152-175
[3] G. Zhu, J. Han, D.Y. Zemlyanov, F.H. Ribeiro, J. Phys. Chem. B 109 (2005) 2331-2337.
[4] F.H. Ribeiro, M. Chow, R.A. Dalla Betta, J. Catal. 146 (1994) 537-544.
[5] K. Fujimoto, F.H. Ribeiro, M. Avalos-Borja, E. Iglesis, J. Catal. 179 (1998) 431-442.
[6] F. Zang, K.L. Hohn, Appl. Catal. B 182 (2016) 570-579.
[7] J. Nilsson, P.-A. Carlsson, N.M. Martin, E.C. Adams, G. Agostini, H. Grönbeck, M. Skoglundh, J. Catal. 356 (2017) 237-345.
[8] M. Santosh Kumar, A. Eyssler, P. Hug, N. van Vegten, A. Baiker, A. Weidenkaff, D. Ferri, Appl. Catal. B 94 (2010) 77-84.
[9] A. Winkler, P. Dimopoulos, R. Hauert, C. Bach, M. Aguirre, Appl. Catal. B 84 (2008) 162-169.
[10] J.B. Miller, M. Malatpure, Appl. Catal. A 495 (2015) 54-62
[11] P. Granger, Y. Renème, A. Lahougue, C. Hamon, F. Dhainaut, Top. Catal. 63 (2020) 1474-1484
[12] Y. Nishihata, J. Mizuki, T. Akao, H. Tanaka, M. Uenishi, M. Kimura, T. Okamoto, N. Hamada, Nature 418 (2002) 164.
[13] M. Uenishi, M. Tanigushi, H. Tanaka, M. Kimura, Y. Nishihata, J. Mizuki, T.Kobayashi, Appl. Catal. B 57 (2005) 267
[14] Y. Lu, K.A. Michalow, M. Santosh Kumar, A. Winkler, A.E. Maegli, S. Yoon, A. Heel, A. Weidenkaff, D. Ferri, Appl. Catal. B144 (2014) 631-643.
[15] P. Pilar Gonzáles-Marcos, B. Pereda-Ayo, A. Aranzabal, J.A. González-Marcos, Catal. Today 180 (2021) 88-95.
[16] Appl. Catal. B 264 (2020) 118475
[17] W.R. Shwartz, L.D. Pfefferle, J. Phys. Chem C 116 (2012) 8571-8579
[18] W.R. Schwartz, D. Ciuparu, L.D. Pferfferle, J. Phys. Chem. C 116 (2012) 8597-8593.
[19] J. Wu, J.-P. Dacquin, N. Djelal, C. Cordier, C. Dujardin, P. Granger, 282 (2021) 119621.
[20] A. Schön, J.-P. Dacquin, P. Granger, C. Dujardin, Appl. Catal. B 223 (2018) 167–176
[21] E. Shustorovich, H. Sellers, Surf. Sci. Rep. 31 (1998) 1-119.
[22] E. Shustorovich, A.T. Bell, Surf. Sci. 289 (1993) 127-138.

[23] H. Stotz, L. Maier, A. Boubnov, A.T. Gremminger, J.-D. Grundwald, O. Deutschmann, J. Catal. 370 (2019) 152-175.
[24] R.S. Monteiro, D. Zemlyanov, J.M. Storey, F.H. Ribeiro, J. Catal. 199 (2001) 291-301.
[25] Y. Wu, C. Dujardin, C. Lancelot, J.P. Dacquin, V. Parvulescu, M. Cabié, C.R. Henry, T. Neisius, P. Granger, J. Catal. 328 (2015) 236-247.
[26] J.P. Dacquin, C. Lancelot, C. Dujardin, P. Granger, J. Phys. Chem. C 115 (2011) 1911-1921.
[27] M. Van den Bossche, H. Grönbeck, J. Am. Chem. Soc. 2015, 137, 12035-12044.